Nuclear Inst. and Methods in Physics Research B 478 (2020) 80–84

Contents lists available at ScienceDirect

Nuclear Inst. and Methods in Physics Research B

journal homepage: www.elsevier.com/locate/nimb

Electronic sputtering of SiC and KBr by high energy ions

N. Matsunami[a,*], S. Okayasu[b], M. Sataka[b], B. Tsuchiya[c]

[a] School of Engineering, Nagoya University, Nagoya 464-8603, Japan
[b] Japan Atomic Energy Agency (JAEA), Tokai 319-1195, Japan
[c] Faculty of Science and Technology, Meijo University, Nagoya 468-8502, Japan

ARTICLE INFO

Keywords:
Electronic sputtering
Lattice disordering
SiC
KBr
Bandgap scheme

ABSTRACT

We have measured electronic sputtering yields of SiC and KBr by high-energy ions (198 MeV Xe, 99 MeV Xe, 89 MeV Ni, 60 MeV Ar and 55 MeV Cl ions with the equilibrium charge). Employing the carbon-foil collector method, sputtered atoms in the C-foil are analyzed by Rutherford backscattering spectrometry (RBS) and the sputtering yields have been evaluated. It appears that the sputtering yields Y follow the power-law of the electronic stopping power (S_e): $Y=(1.86S_e)^{1.53}$ and $Y=(0.77S_e)^{3.0}$ for SiC and KBr, respectively (S_e in keV/nm). The representative sputtering yield at S_e = 10 keV/nm is evaluated to be 87.6 and 457 for SiC (bandgap E_g = 2.86 eV) and KBr (E_g = 7.4 eV) and it is revealed that these can be explained within the bandgap scheme. Lattice disordering by ion impact has been also measured by X-ray diffraction (XRD) and S_e dependence of the XRD intensity degradation is compared with that of electronic sputtering.

1. Introduction

Electronic sputtering representing atomic displacement near surface caused by electronic excitation under high-energy ion irradiation has been observed for many non-metallic solids, e.g., H_2O ice [1,2], frozen gas films of Xe, CO_2 and SF_6 [2], those of Ar, N_2 and CO [3], SiO_2 and Si_3N_4 [4], UF_4 and UO_2 [5], UO_2 [6], LiF [7,8], SiO_2 [7,9,10], $SrCeO_3$ and $SrTiO_3$ [9], CeO_2, Al_2O_3, MgO, TiO_2 and ZnO [11], crystalline SiO_2 and comparison with SiO_2-glass [12,13], $MgAl_2O_4$ [12], AlN, Si_3N_4, Y_2O_3 and ZrO_2 [14], Cu_2O [15], Cu_3N [16], CuO [17], WO_3 [18], Fe_2O_3 [19], and WNO_x ($x\approx0.4$) [20]. Nearly stoichiometric sputtering has been reported [7,9,11,14,17–20], while considerable deviation has been reported for $YBa_2Cu_3O_7$ [21], $Gd_3Ga_5O_{12}$ and $Y_3Fe_5O_{12}$ [22], and CaF_2 and UF_4 [23]. Only heavy elements [4–6] or light element [10] have been measured. Besides electronic sputtering, material modification by ion irradiation has been observed, e.g., track formation in mica etc. [24], mica, SiO_2, Al_2O_3 etc. [25], Si_3N_4 [26], lattice disordering (i.e., degradation of X-ray diffraction (XRD) intensity) and lattice expansion for polycrystalline films of SiO_2 [27], WO_3 [18], disordering of ultra thin films of WO_3 [28], disordering and lattice compaction for polycrystalline films of Cu_2O [15], Cu_3N [16], CuO [17], Fe_2O_3 [19], Mn-doped-ZnO [29]. Peculiarly, lattice expansion and compaction at low and high ion fluence as well as disordering have been reported for WNO_x films [20]. Furthermore, drastic decrease of the electrical resistivity has been observed for Cu_3N [16], WNO_x [20] and Mn-doped-ZnO [29].

Three models have been discussed for electronic-excitation induced atomic displacement, Coulomb explosion (CE) model [24], thermal spike (TS) model [7] and exciton model that non-radiative decay of self-trapped exciton (STX, i.e., localized excited state coupled with lattice) leads to atomic displacement [3,30–34]. Since, the fraction of sputtered ions for 100 MeV Xe ions on SiO_2 glass is small [12], CE model is unsound. According to a crude estimation based on TS model, evaporation yield of SiO_2 is far smaller than the experimental value [14], and thus TS model neither sound. Moreover, transfer mechanism from the electronic energy into lattice (electron-lattice coupling) is not clear in the model. According to the STX model or bandgap scheme, it is anticipated that the energy of atoms in motion from non-radiative decay of the electronic excited state coupled with the lattice is comparable with the bandgap, resulting in larger sputtering yield with larger bandgap and this seems to be supported by the experimental results for the bandgap larger than 3 eV [19]. However, a drawback of this model is that existence of STX is known for limited materials, rare gas solids, SiO_2, Al_2O_3, MgO, alkali halides etc. [3,33–34] and does not exist in MgO and probably in Al_2O_3 [35]. A conflict is seen in refs. [33] and [35], and the opinion of ref. [35] is favored in view of radiation sensitivity. Alternatively, a mechanism is suggested for coupling of exited state with lattice via Coulomb repulsion during neutralization time of ~fs [19]. To examine the suggested mechanism, more data is desired for materials other than oxides, nitrides.

* Corresponding author.
E-mail address: n-matsunami@nucl.nagoya-u.ac.jp (N. Matsunami).

https://doi.org/10.1016/j.nimb.2020.05.003
Received 20 November 2019; Received in revised form 28 April 2020; Accepted 3 May 2020

In this paper, the electronic sputtering yields of SiC and KBr have been measured and the bandgap scheme for the electronic sputtering has been discussed. SiC has been chosen because of availability of samples and no publication of electronic sputtering of carbides, and KBr because of lack of electronic sputtering data and interest of comparison with the electronic sputtering yields of LiF [7,8]. Furthermore, lattice disordering induced by ions is measured and compared with the electronic sputtering.

2. Experimental

Commercially available samples of hexagonal-SiC with c-axis orientation (CREE Wafer Products, 0.2 mm thickness) and face-centered-cubic KBr (1 0 0) single crystal (Harshaw products, cleaved to sub mm thickness before ion irradiation) are employed. Irradiation of high-energy ions (200 MeV Xe^{+14}, 100 MeV Xe^{+14}, 90 MeV Ni^{+10}, 60 MeV Ar^{+7} and 55 MeV Cl^{+7}) have been performed at room temperature and normal incidence by using the Tandem accelerator at Japan Atomic Energy Agency (JAEA). Sample orientation is not intentionally aligned to major axis of samples in order to avoid the channeling effect. Moreover angular spread of approximately a half of degree under scanning of beams for attaining beam uniformity is comparable with the channeling critical angle of 0.32 deg. (SiC, along ⟨0 0 1⟩) and 0.65 deg. (KBr) for 100 MeV Xe ion calculated by Lindhard's formula, $(2Z_1Z_2e^2/Ed)^{1/2}$ [36], reducing the channeling effect. Here, Z_1 is the atomic number of the ion, Z_2 mean atomic number of samples, e the charge of an electron, E the ion energy, d the atomic spacing of the channeling axis. For calculation of the critical angle, d equal to the lattice parameter of c-axis is taken to be 0.504 nm for SiC [37] and d (=half of the lattice parameter) 0.33 nm for KBr [38]. The lattice parameters are confirmed by XRD with Cu-k_α. The beam current density is ~3nA cm^{-2} for high-energy ions and the corresponding temperature-rise during the ion irradiation is estimated to be less than 40 °C [39], which is not significant.

Carbon-foil-collector method [9] is applied to obtain sputtering yields for high-energy ions, i.e., samples are irradiated by high-energy ions after passing through the carbon-foil (100 nm)-collector, and sputtered atoms are collected in the C-foil followed by RBS of 1.5 and 1.8 MeV He^+ ions. During passing through the C-foil, the ions attain the equilibrium charge. The energy loss in the C-foil is calculated to be 2, 1, 1 MeV for 200 MeV Xe, 100 MeV Xe and 90 MeV Ni, and less than 1 MeV for 60 MeV Ar and 55 MeV Cl, using TRIM 1997 [40] and these energy losses are insignificant. 120 keV Ne ions by a 200 kV accelerator at Nagoya University, are employed to obtain the collection efficiency of K and Br. Density of Si (SiC, 3.16 g cm^{-3}) and Br (KBr, 2.74 gcm^{-3}) is taken to be 4.75 and 1.387 × 10^{22} cm^{-3} [41] for stopping power calculation [40] required for ion beam analysis.

3. Results and discussion

Fig. 1(a) shows the amount of sputtered Si collected in C-foil from SiC vs ion fluence, noticing that sputtered C is unable to detect. It appears that the Si areal density is proportional to the ion fluence, indicating negligible overlapping effect. From the slope of the Si areal density vs ion fluence with the collection efficiency of 0.48 for Si [9], sputtering yields are evaluated. Here, stoichiometric sputtering is assumed, taking the experimental results into account that the composition ratio of C over Si for both irradiated after 200 MeV Xe at 3.7 × 10^{12} cm^{-2} and unirradiated part of SiC is found to be close to unity by 1.5 MeV He RBS with the RBS accuracy of 10%. Thus, total sputtering yield of SiC is twice of Si sputtering yield and the results are summarized in Table 1. Sputtering yields by high-energy ions are much larger than those calculated based on the elastic collisions (proportional to the nuclear stopping power), indicating that for high-energy ions, the electronic excitation plays a major role.

The XRD intensity (diffraction angle 2θ of 35.6 °, (0 0 2) diffraction)

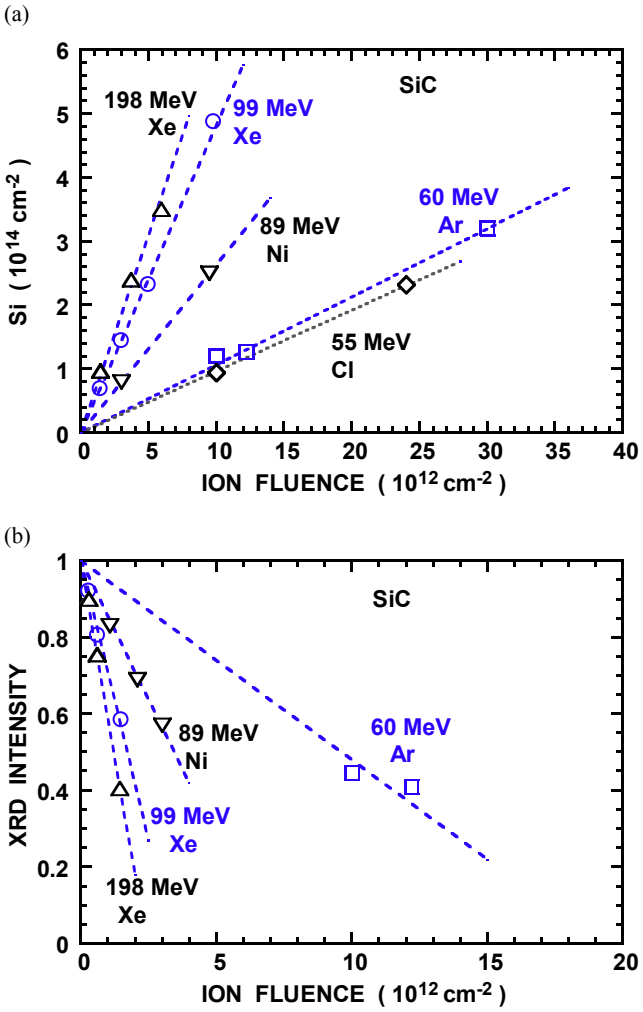

Fig. 1. (a) Areal density of Si (10^{14} cm^{-2}) collected in C-foil sputtered from SiC, (b) XRD intensity of SiC vs ion fluence (10^{12} cm^{-2}) for 198 MeV Xe (▲), 99 MeV Xe (◯), 89 MeV Ni (▽), 60 MeV Ar (□) and 55 MeV Cl (◇) ions with the equilibrium charge. An estimated error of the areal density and XRD intensity is 10%.

relative to that of unirradiated SiC vs ion fluence is shown in Fig. 1(b) and it is seen that the XRD intensity degradation linearly depends on the ion fluence. Similarly to the sputtering yield evaluation, the XRD intensity degradation (Y_D) per ion fluence is obtained from the slope and the results are given in Table 1. Here, the X-ray attenuation length (ℓ) is obtained to be 69 μm [42] and the attenuation depth (ℓ sinθ) 21 μm. Thus the electronic stopping power is averaged over the depth of d_{XP} (S_e^{av}) such that (S_e at depth d_{XP} / S_e at surface) ●exp(-2 d_{XP} /ℓ sinθ) is less than 20%, meaning that XRD contribution at depth d_{XP} is less than 20% and S_e being the electronic stopping power. As described below, the contribution is much less than 20%, since Y_D super-linearly depends on S_e or S_e^{av}. S_e^{av} and d_{XP} are given in Table 1. Sputtering yield Y and Y_D vs S_e are shown in Fig. 2. Y and Y_D are found to follow power law: $Y=(1.86S_e)^{1.53}$, $Y_D=(0.0287S_e)^{1.73}$ and $Y_D=(0.037\ S_e^{av})^{1.97}$ as shown in Fig. 2. S_e dependence of Y and Y_D is similar, but the exponent of the XRD degradation is slightly larger than that of sputtering. This difference could be partly due to the fact that smaller displacement and thermal annealing are involved in the lattice disordering.

RBS spectrum of C-foil after irradiation by 90 MeV Ni ions on KBr is shown in Fig. 3(a). Br peak without appreciable background is observed in the RBS and K spectrum is partly overlapped with Cl (probably due to NaCl contamination). It appears that the areal density of K is larger by a factor of 2–4 than that of Br. This implies, comparing with the

Table 1
Electronic (S_e), nuclear (S_n) stopping powers (keV/nm) near surface of SiC and KBr, and projected range (R_p) for 198 MeV ^{136}Xe, 99 MeV ^{136}Xe, 89 MeV ^{58}Ni, 60 MeV Ar^{+7} and 55 MeV Cl^{+7} ions calculated using TRIM1997 [40] and sputtering yield Y (per ion) of SiC and KBr. S_e^{av} is the electronic stopping power averaged over the depth of d_{XP} relevant to XRD and Y_D the XRD intensity degradation.

Ions	S_e	S_n	R_p	Y	S_e^{av}	d_{XP}	Y_D
	(keV/nm)		(μm)		(keV/nm)	(μm)	(10^{-12}cm^2)
SiC							
198 MeV Xe	20.74	0.0735	15.3	258	17.62	10.5	0.41
99 MeV Xe	17.2	0.129	10.2	200	13.53	6.5	0.29
89 MeV Ni	11.35	0.0207	10.3	110	9.91	8.5	0.145
60 MeV Ar	6.4	0.00924	10.5	44.4	5.97	9.2	0.052
55 MeV Cl	6.1	0.00794	10.1	40.0			
KBr							
198 MeV Xe	12.38	0.0508	27	713	11.63	8	2.35
99 MeV Xe	9.7	0.089	18.3	500	8.5	8	1.3
89 MeV Ni	6.81	0.014	18.3	113	6.64	8	0.64
55 MeV Cl	3.65	0.0053	17.9	30			

collection efficiency of Br (0.4) as described later, that the collection efficiency of K in the C-foil collector exceeds unity and this is unrealistic. Based on these results, Br yields with an assumption of stoichiometric sputtering are employed to obtain the total sputtering yield of KBr, considering that the composition ratio of K over Br for both the unirradiated part and irradiated part of KBr by 100 MeV Xe at 2.6×10^{12} cm^{-2} is found to be close to unity by 1.5 MeV He RBS.

The amount of sputtered Br from KBr vs ion fluence is shown in Fig. 3(b). It also appears that the Br areal density is proportional to the ion fluence, indicating that the overlapping effect is not appreciable. From the slope of the Br areal density vs ion fluence with the collection efficiency of 0.4 for Br with assumption of stoichiometric sputtering, sputtering yields are evaluated and the results are given in Table 1. Here, the collection efficiency of Br in the C (100 nm) -foil is obtained to be 0.4 as follows. The geometrically same set of C-foil and KBr is irradiated by 120 keV Ne ions. The energy loss in the C-foil is calculated to be 60 keV [40]. Sputtering yields of 60 keV Ne on KBr is estimated to be 0.672, assuming that the elastic sputtering yield is proportional to the nuclear stopping power [40] with the experimental value of 1.9 for 8 keV Ar [43]. The collection efficiency is given by the areal density of Br times components number (2) divided by (Ne ion fluence times sputtering yield of 60 keV Ne). We adopt the sputtering data [43] because the sputtering yield by 60 keV Ne for KBr is estimated to be 0.2 from [44] and this value is smaller by a factor of 3 than the value mentioned above, implying that the collection efficiency is larger than unity. As in the case of SiC, sputtering yields by high-energy ions are much larger than those calculated based on the elastic collisions, indicating that for high-energy ions, the electronic excitation plays a major role.

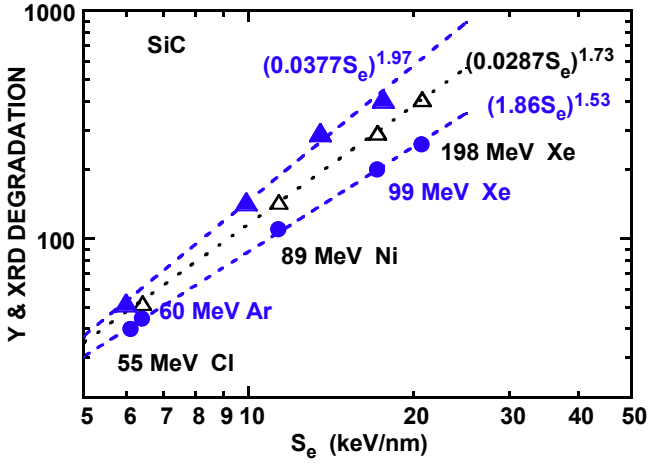

Fig. 2. Sputtering yield per ion Y (●) and XRD intensity degradation Y_D (10^{-15} cm^2) (△) as a function of the electronic stopping power (S_e (keV/nm)), and Y_D vs S_e^{av} (▲). An estimated error of Y and Y_D is 10%.

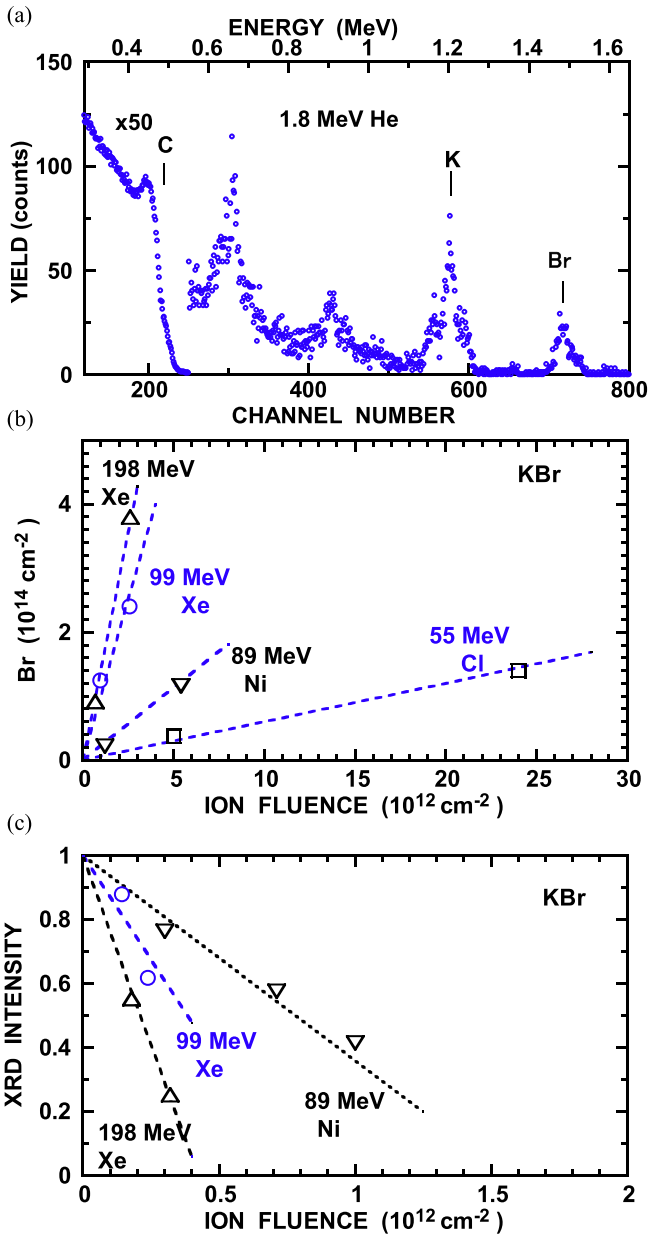

Fig. 3. (a) RBS of C-foil (placed on graphite sheet of ~1 mm thickness) collected K and Br sputtered from KBr after irradiation of 90 MeV Ni ions at 5.4×10^{12} cm^{-2}, obtained by 1.8 MeV He^+ and normal incidence with the scattering angle of 160 deg. Carbon edge and peaks of K and Br are indicated by vertical lines. Peaks around 0.67, 0.9 and 1.16 MeV are identified as oxygen, Na and Cl. (b) Areal density of Br (10^{14} cm^{-2}) collected in C-foil sputtered from KBr, (c) XRD intensity of KBr vs ion fluence (10^{12} cm^{-2}) for 198 MeV Xe (▲), 99 MeV Xe (●), 89 MeV Ni (▽) and 55 MeV Cl (□) ions with the equilibrium charge. An estimated error of the areal density and XRD intensity is 20%.

The XRD intensity (diffraction angle 2θ of 27 °, (0 0 2) diffraction) relative to that of unirradiated KBr vs ion fluence is shown in Fig. 3(c) and ion fluence dependence of the XRD intensity degradation is found to be linear. The XRD intensity degradation (Y_D) per ion fluence is obtained from the slope and the results are given in Table 1. Here, the

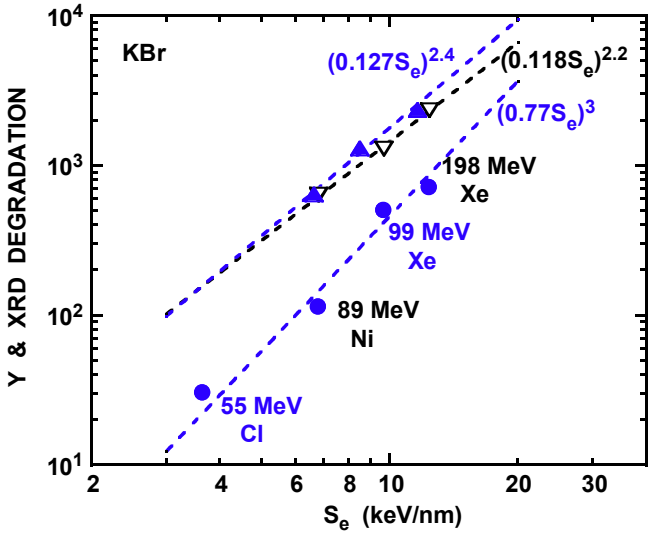

Fig. 4. Sputtering yield per ion Y (●) and XRD intensity degradation Y_D (10^{-15} cm^2) (▽) as a function of the electronic stopping power (S_e (keV/nm)), and Y_D vs S_e^{av} (▲). An estimated error of Y and Y_D is 20%.

X-ray attenuation length (ℓ) and depth (ℓ sinθ) are obtained to be 34 μm [42] and 8 μm. Since the projected range (Table 1) is larger than the attenuation depth, S_e^{av} is averaged over the depth of d_{XP} = 8 μm so that (S_e at depth d_{XP} / S_e at surface) ●exp(-2 d_{XP} /ℓ sinθ) is less than 10%, meaning that XRD contribution is less than 10%. As described below, the contribution is much less than 10%, since Y_{XD} super-linearly depends on S_e or S_e^{av}. S_e^{av} and d_{XP} are given in Table 1. Sputtering yield Y and Y_D vs S_e are shown in Fig. 4. Y and and Y_D are found to follow power law: $Y=(0.77S_e)^{3.0}$, $Y_D=(0.\ 118S_e)^{2.2}$ and $Y_D=(0.127\ S_e^{av})^{2.4}$ as shown in Fig. 4. For S_e dependence of Y and Y_D, the exponent of the XRD degradation is a little bit smaller than that of electronic sputtering, and this trend is opposite to SiC results. These could be partly due to the fact that smaller displacement and thermal annealing are involved in the lattice disordering. More data would be desired to investigate the correlation between the electronic sputtering and lattice disordering.

Representative sputtering yield at S_e = 10 keV/nm vs bandgap (E_g) is shown in Fig. 5 for SiC (Y = 88) and KBr (Y = 457) as well as published data [19]. Bandgap is taken to be 2.86 eV (SiC) [37], 7.4 eV (KBr) [45]. Also shown is the LiF data (Y = 480 [8] and E_g = 13.6 eV

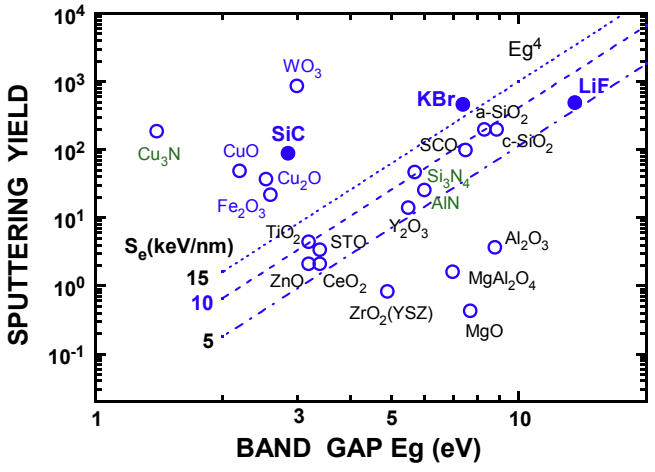

Fig. 5. Sputtering yields at S_e = 10 keV/nm vs bandgap, E_g (eV) for SiC and KBr (●), other data [19] and LiF (●) [8]. E_g dependence of the upper limit of the sputtering yields at S_e = 10 keV/nm is indicated by dash line for E_g > 3 eV. Similarly, E_g dependence is shown for S_e = 15 keV/nm (dot line) and 5 keV/nm (dot-dash line).

[45]) after correcting for normal incidence and total (Li and F) yield. The results of KBr and LiF are comparable with the fit to the upper limit to the published data of oxides and nitrides (E_g^4 dependence as illustrated by the dash line in Fig. 5) based on the bandgap scheme [19], which will be discussed in the next paragraph, though the KBr result is somewhat larger than the expected value from the fit and the bandgap dependence is much weaker for alkali halides, KBr and LiF. This weak dependence could be partly due to material dependence of anisotropic component anticipated for alkali halides and the fact that the sticking coefficient of Li and F on the collector is taken to be unity for LiF [7,8], and more data is desired to resolve the issue. The yield of SiC is larger than the value anticipated from the fit, though deviation is not as much as for exceptionally large yield of WO_3 and this is also to be investigated. It is noticed that some data scatter (SiO_2, MgO and Al_2O_3 with nearly the same bandgap) can be explained by whether STX exists or not, as mentioned in Introduction and [14]. In Fig. 5, sputtering data of Cu_2O [15] has been reanalyzed and revised as Y = $3.67S_e$. Revised value is 18 at S_e = 10 keV/nm. Similarly to SiC and KBr, the composition ratio of O over Cu is found to be nearly 0.5 by 1.8 MeV He RBS for both irradiated part by 90 MeV Ni at 2 × 10^{12} cm^{-2} and unirradiated part. Also, sputtering data of Cu_3N [16] has been reanalyzed and revised as Y = 960, 556, 342 and 142 at S_e (keV/nm) = 27.34, 20.74, 15.0 and 8.47 for 198 MeV Xe, 99 MeV Xe, 89 MeV Ni and 60 MeV Ar ions, respectively. The power-law fit remains the same, $Y=(2.6\ S_e)^{1.6}$. The composition ratio of N over Cu is found to be nearly 1/3 by 1.8 MeV He RBS for both irradiated part by 90 MeV Ni at 1.4 × 10^{12} cm^{-2} and unirradiated part.

Now, a suggested mechanism of electron-lattice coupling [19] is briefly described. A dense ionized core is generated by high-energy ion impact and Coulomb repulsion leads to atomic motion. Generally, neutralization time is too short so that CE model is not adequate to explain the electronic sputtering. Nevertheless, displacement of one tenth of the nearest neighbor distance (~0. 1 nm) is highly achievable during the short neutralization time (~fs). As the first step, using a formula [46], time required for Si^+-C^+ separation (0.01 nm) is estimated to be 6 fs, and 9 fs for K^+-Br^+. This comes up to suggestion [19] that small atomic displacements lead to electron-lattice coupling, generation of highly excited-state coupled with lattice (h-ESCL). Non-radiative decay h-ESCL leads to atomic displacement (larger displacements result in sputtering and smaller displacements end up generation of phonons or lattice distortion). For KBr, non-radiative decay of STX near room temperature is dominant over radiative decay [47]. It also has been argued that multi-exciton such as bi-self-trapped-exciton, a form of h-ESCL leads to more efficient non-radiative decay [48]. In addition, the effective depth contributing to the electronic sputtering of WO_3 has been obtained to be 40 nm for both 99 MeV Xe and 89 MeV Ni ions and it turns out to be that the energy deposition within the effective depth is adequate for explaining the sputtering yield [49]. Quantitative argument is desired for efficiency of h-ESCL generation, branching ratio of non-radiative decay and fraction of larger atomic displacement leading to sputtering.

4. Summary

The electronic sputtering yields Y of SiC and KBr have been measured and Y fits to the power law formula: $Y=(1.86S_e)^{1.53}$ and $Y=(0.77S_e)^{3.0}$, respectively, S_e being the electronic stopping power (keV/nm). It appears that the sputtering yield can be explained within the bandgap scheme that non-radiative decay of highly excited-states coupled with lattice assisted with Coulomb repulsion in the dense ionized core along high-energy ion path during the neutralization time leads to atomic displacement. Lattice disordering by ion irradiation have been measured and XRD intensity degradation per fluence Y_D fits to power law formula: $Y_D = (0.0377S_e^{av})^{1.97}$ and $(0.127S_e^{av})^{2.4}$ for SiC and KBr, respectively, S_e^{av} being the electronic stopping power averaged over the depth relevant to XRD. The exponent of sputtering and

disordering are comparable, implying that the similar mechanism is involved in sputtering and disordering.

Declaration of Competing Interest

The authors declare that they have no known competing financial interests or personal relationships that could have appeared to influence the work reported in this paper.

Acknowledgement

XRD is performed at Radioisotope Research Center, Nagoya University. This work was partly supported by the Cooperative Research Program of JAEA and University of Tokyo.

References

[1] W.L. Brown, L.J. Lanzerotti, J.M. Poate, W.M. Augustyniak, Phys. Rev. Lett. 40 (1978) 1027.
[2] J. Bottiger, J.A. Davies, J. L'Ecuyer, N. Matsunami, R. Ollerhead, Rad. Eff. 49 (1980) 119.
[3] W.L. Brown, L.J. Lanzerotti, K.J. Marcantonio, R.E. Johnson, C.T. Reimann, Nucl. Instru. Meth. B14 (1986) 392.
[4] Y. Qiu, J.E. Griffith, W.J. Meng, T.A. Tombrello, Rad. Eff. 70 (1983) 231.
[5] C.K. Meins, J.E. Griffith, Y. Qiu, M.H. Mendenhall, L.E. Seiberling, T.A. Tombrello, Rad. Eff. 71 (1983) 13.
[6] S. Bouffard, J.P. Duraud, M. Mosbah, S. Schlutig, Nucl. Instru. Meth. B 141 (1998) 372.
[7] M. Toulemonde, W. Assmann, C. Trautmann, F. Gruner, Phys. Rev. Lett. 88 (2002) 057602.
[8] W. Assmann, B.B. -d'Etat, M. Bender, P. Boduch, P.L. Grande, H. Lebius, D. Lelievre, G.G. Marmitt, H. Rothard, T. Seidl, D. Severin, K.-O. Voss, M. Toulemonde, C. Trautmann, Nucl. Instrum. Meth. B 392 (2017) 94.
[9] N. Matsunami, M. Sataka, A. Iwase, Nucl. Instru. Meth. B193 (2002) 830.
[10] W.M. Arnoldbik, N. Tomozeiu, F.H.P.M. Habraken, Nucl. Instru. Meth. B 203 (2003) 151.
[11] N. Matsunami, M. Sataka, A. Iwase, S. Okayasu, Nucl. Instru. Meth. B 209 (2003) 288.
[12] N. Matsunami, O. Fukuoka, T. Shimura, M. Sataka, S. Okayasu, Nucl. Instru. Meth. B 230 (2005) 507.
[13] M. Toulemonde, W. Assmann, C. Trautmann, Nucl. Instru. Meth. B 379 (2016) 2.
[14] N. Matsunami, M. Sataka, S. Okayasu, M. Tazawa, Nucl. Instru. Meth. B 256 (2007) 333.
[15] N. Matsunami, M. Sataka, S. Okayasu, N. Ishikawa, M. Tazawa, H. Kakiuchida, Nucl. Instru. Meth. B 266 (2008) 2986.
[16] N. Matsunami, H. Kakiuchida, M. Tazawa, M. Sataka, H. Sugai, S. Okayasu, Nucl. Instru. Meth. B 267 (2009) 2653.
[17] N. Matsunami, Y. Sakuma, M. Sataka, S. Okayasu, H. Kakiuchida, Nucl. Instru. Meth. B 314 (2013) 55.
[18] N. Matsunami, M. Sataka, S. Okayasu, H. Kakiuchida, Nucl. Instru. Meth. B 268 (2010) 3167.
[19] N. Matsunami, S. Okayasu, M. Sataka, Nucl. Instru. Meth. B 435 (2018) 142.
[20] N. Matsunami, S. Okayasu, M. Sataka, B. Tsuchiya, Nucl. Instru. Meth. B 435 (2018) 146.
[21] N. Matsunami, M. Sataka, A. Iwase, Nucl. Instru. Meth. B175–177 (2001) 56.
[22] A. Meftah, W. Assmann, N. Khalfaoui, J.P. Stoquert, F. Studer, M. Toulemonde, C. Trautmann, K.-O. Voss, Nucl. Instru. Meth. B 269 (2011) 955.
[23] M. Toulemonde, W. Assmann, D. Muller, C. Trautmann, Nucl. Instru. Meth. B 406 (2017) 501.
[24] R.L. Fleischer, P.B. Price, R.M. Walker, J. Appl. Phys. 36 (1965) 3645.
[25] M. Toulemonde, S. Bouffard, F. Studer, Nucl. Instru. Meth. B91 (1994) 108.
[26] K. Nakajima, Y. Morita, M. Suzuki, K. Narumi, Y. Saitoh, N. Ishikawa, K. Hojou, M. Tsujimoto, S. Isoda, K. Kimura, Nucl. Instru. Meth. B291 (2012) 12.
[27] N.S. Shinde, N. Matsunami, T. Shimura, M. Sataka, S. Okayasu, T. Kato, M. Tazawa, Nucl. Instru. Meth. B245 (2006) 231.
[28] N. Matsunami, M. Kato, M. Sataka, S. Okayasu, Nucl. Instru. Meth. B409 (2017) 272.
[29] N. Matsunami, M. Itoh, M. Kato, S. Okayasu, M. Sataka, H. Kakiuchida, Nucl. Instru. Meth. B365 (2015) 191.
[30] N. Itoh, Adv. Phys. 31 (1982) 491.
[31] N. Itoh, A.M. Stoneham, Nucl. Instru. Meth. B146 (1998) 362.
[32] K.S. Song, R.T. Williams, Self-Trapped Excitons, second ed., Springer-Verlag, Berlin, 1996.
[33] N. Itoh, A.M. Stoneham, Materials Modification by Electronic Excitation, Cambridge University Press, 2001.
[34] D.M. Duffy, S.L. Daraszewicz, J. Mulroue, Nucl. Instru. Meth. B 277 (2012) 21.
[35] P. Martin, S. Guizard, Ph. Daguzan, G. Petite, P. D'Oliveira, P. Meynadier, M. Perdix, Phys. Rev. B 55 (1997) 5799.
[36] J.R. Tesmer, M. Nastasi (Eds.), Handbook of Modern Ion Beam Materials Analysis, Materials Research Society, Pittsburgh, 1995, Chap. 10.
[37] W. Martienssen, H. Warlimont (Eds.), Handbook of Condensed Matter and Materials Data, Springer, Berlin, 2005.
[38] C. Kittel, Introduction to Solid State Physics, fifth ed., John Wiley & Sons, New York, 1976.
[39] N. Matsunami, T. Yajima, H. Iwahara, Nucl. Instrum. Meth. B 65 (1992) 278.
[40] J.F. Ziegler, J.P. Biersack, U. Littmark, The Stopping and Range of Ions in Solids, Pergamon Press, New York, 1985.
[41] D.R. Lide (Ed.), CRC Handbook of Chemistry and Physics, 84th ed., CRC Press, New York, 2003.
[42] E. Storm, H.I. Israel, Nucl. Data Tables A7 (1970) 565.
[43] S.V. Barbashev, N.A. Poklonova, T.B. Shashkina, All-Russian Conf., 1978, Minsk, in: R. Behrisch (Ed.), Sputtering by Particle Bombardment II, Springer-Verlag, Berlin, 1983.
[44] B. Navinsek, J. Appl. Phys. 36 (1965) 1678.
[45] J.T. Devreese, A.B. Kunz, T.C. Collins, Solid State Commu. 11 (1972) 673.
[46] D.S. Gemmell, Chem. Rev. 80 (1980) 301.
[47] K. Tanimura, J. Phys. C: Solid State Phys. 11 (1978) 3835.
[48] N. Matsunami, H. Hosono, Phys. Rev. B 60 (1999) 10616.
[49] N. Matsunami, M. Sataka, S. Okayasu, Nucl. Instrum. Meth. B460 (2019) 185.